Environmental Technology

ISSN: 0959-3330 (Print) 1479-487X (Online) Journal homepage: www.tandfonline.com/journals/tent20

Experimental study on enrichment of heavy metals by modified mullite during co-combustion of lignite with eucalyptus wood

Jingjing Li, Zhaosheng Yu, Jinxi Dong, Zi You, Wen Teng & Xiaoqian Ma

To cite this article: Jingjing Li, Zhaosheng Yu, Jinxi Dong, Zi You, Wen Teng & Xiaoqian Ma (2025) Experimental study on enrichment of heavy metals by modified mullite during co-combustion of lignite with eucalyptus wood, Environmental Technology, 46:12, 2052-2063, DOI: 10.1080/09593330.2024.2417316

To link to this article: https://doi.org/10.1080/09593330.2024.2417316

ENVIRONMENTAL TECHNOLOGY
2025, VOL. 46, NO. 12, 2052–2063
https://doi.org/10.1080/09593330.2024.2417316

Taylor & Francis
Taylor & Francis Group

Experimental study on enrichment of heavy metals by modified mullite during co-combustion of lignite with eucalyptus wood

Jingjing Li[a,b], Zhaosheng Yu [a,b], Jinxi Dong[a,b], Zi You[a,b], Wen Teng[a,b] and Xiaoqian Ma [a,b]

[a]School of Electric Power, South China University of Technology, Guangzhou, People's Republic of China; [b]Guangdong Key Laboratory of Efficient and Clean Energy Utilization Institutes, School of Electric Power, South China University of Technology, Guangzhou, People's Republic of China

ABSTRACT

Modifying the content of oxygen vacancies (OVs) has emerged as a crucial approach to tailoring silicate's adsorption properties, microstructure, conductivity, and catalytic performance. Some studies have reported the formation of OVs during ammonia treatment. However, there are limited studies on the production of OV-enriched mullite by treating it with N-containing compounds at low temperatures. In this work, formamide, urea, and ammonium acetate were used as ammonia-assisted reduction modifiers to induce oxygen vacancies in mullite at 30 °C, 60 °C, and 90 °C. The aim was to enhance the enrichment effect of heavy metals (Cr, Cu, Mn, Ni, Pb, Zn) during the co-combustion of coal and biomass. The modified mullite was analyzed by using X-ray diffraction (XRD), Brunauer-Emmett-Teller (BET) surface area analysis, scanning electron microscopy (SEM), and Fourier transform infrared spectroscopy (FTIR). The results indicated that the particle size of mullite decreased, and the concentration of internal Al^{3+} ions and oxygen vacancies was enhanced. Coal-biomass-mullite combustion experiments were conducted in a tubular furnace at 900 °C, revealing a significant enhancement in the enrichment of heavy metals during the combustion process, particularly when the modification temperature was 60 °C using ammonium acetate as the modifier. This work holds significant importance for developing novel heavy metal adsorbents and the reduction of pollutant emissions from coal-biomass co-combustion in industrial applications.

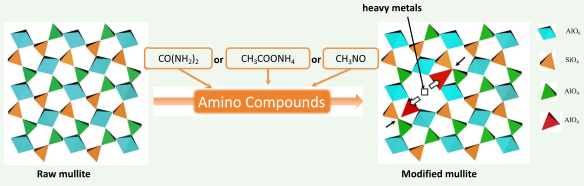

ARTICLE HISTORY
Received 23 May 2024
Accepted 27 September 2024

KEYWORDS
Co-combustion; oxygen vacancy; mullite; enrichment; heavy metal

1. Introduction

With the increasing global energy demand and worsening environmental issues, co-combustion of coal and biomass has attracted significant attention. This technology utilizes renewable biomass resources to replace or supplement coal, thereby reducing the consumption of fossil fuels and improving energy utilization efficiency. Studies have shown that co-combustion can significantly reduce emissions of NO_X and CO_2 [1–3], and increasing the biomass content can further enhance emission reduction effects [4–6], improve air quality and environmental health, and promote sustainable development. However, heavy metal elements in coal and biomass pose potential threats to the environment and human health. Some of these compounds have been classified as carcinogens by the International Agency for Research on Cancer (IARC), a subsidiary of the World Health Organization.

With the exacerbation of urbanization and industrialization, the release of heavy metals poses a threat to human health and ecosystems, the stabilization and solidification of heavy metals become crucial [7]. There are many methods to remove heavy metals from wastewater [8–10]. Among them, adsorption method has attracted much attention and become the mainstream method [11,12]. Various materials have been developed for removing heavy metals from boiler combustion, such as activated carbon, zeolites, carbon nanotubes,

CONTACT Zhaosheng Yu zsyu@scut.edu.cn School of Electric Power, South China University of Technology, 510640, Guangzhou, People's Republic of China; Guangdong Key Laboratory of Efficient and Clean Energy Utilization Institutes, School of Electric Power, South China University of Technology, No. 381, Wushan Road, Tianhe District, 510640, Guangzhou, People's Republic of China

Supplemental data for this article can be accessed online at https://doi.org/10.1080/09593330.2024.2417316.

graphene, etc. [13–15]. The addition of aluminosilicates to the coal combustion process is a feasible and promising technique for emission control. Studies have shown that Si/Al-based compounds can form stable complexes with heavy metals.

Mullite, a natural mineral first discovered on the Isle of Mull in Western Scotland, is an exceedingly rare compound in nature [16]. It composes $3Al_2O_3{:}2SiO_2$ and represents a stable compound within the Al_2O_3-SiO_2 system. Owing to its distinct crystal structure and exceptional high-temperature resistance, which have garnered extensive investigations within the realms of environmental science and materials engineering. Its outstanding thermal stability and mechanical strength have rendered it highly coveted in these fields [17]. The crystal structure of mullite can be derived from sillimanite (chemical composition: Al_2SiO_5, $x = 0.00$), as depicted in Figure 1. Mullite evolves from sillimanite through a coupled substitution mechanism involving the conversion of $2Si^{4+}+O^{2-}\rightarrow 2Al^{3+}+\square$ ($\square =$ oxygen vacancy) [17]. The oxygen atom O* that connects the two tetrahedral is removed during this process. Simultaneously, the tetrahedral cations associated with these oxygen atoms are repositioned to positions labelled as T*. This rearrangement results in the formation of T_3O groups (also referred to as triclusters). The number of oxygen vacancies directly corresponds to the value of x in the mullite solid solution series $Al_{4+2x}Si_{2-2x}O_{10-x}$ [18] ($\approx 0.2 < x < 0.67$ [19]).

Current research indicates that pure silica-alumina mordenite possesses theoretical potential for treating heavy metal pollution due to its unique microstructure and physicochemical properties [20]. Numerous studies have shown that a few metal cations, including Fe^{3+}, Ti^{4+}, Cr^{3+}, V^{3+}, Cu^{2+}, etc, can be incorporated into natural/synthetic mullite [19,21]. These cations predominantly replace Al^{3+} in the octahedral positions [22,23], with a smaller degree of substitution occurring in the tetrahedral positions [24,25]. The control of foreign cation doping is influenced by various factors, including their oxidation state and ionic radius, as well as the temperature, pressure, and chemical environment during the doping process. Additionally, ions such as Pb^{2+}, Cd^{2+}, Co^{2+}, Ni^{2+}, and Zn^{2+} can serve as charge compensators, filling oxygen vacancies, neutralizing negative charges [26,27]. Furthermore, oxygen vacancies can promote the reduction of heavy metals and hinder their participation in biogeochemical cycles, thereby reducing the risks associated with these heavy metals [28,29]. To enhance the effectiveness of mullite in heavy metal removal, methods such as laser irradiation [30], ion doping [31], etching [32], reduction [33], and heat treatment [34] can be used to increase the oxygen vacancy content in the structure. Guo et al. synthesized Co_3O_4 nanosheets with varying levels of oxygen vacancies by conducting hydrogen/nitrogen reduction at 200 °C [35]. Moreover, Qu et al. employed urea to modify Cu-Mn oxide catalysts, inducing the formation of oxygen vacancies through the ammonia generated from urea pyrolysis [36]. Furthermore, Yu et al. demonstrated an enhancement in oxygen vacancy concentration and catalytic activity by reducing MnO_2 with $NaBH_4$ [37]. Studies have demonstrated that sodium borohydride and hydrazine are capable of inducing vacancy defects on material surfaces [38]. Inspired by these researches, an attempt can be made to adjust the oxygen vacancy content in mullite by using N-containing compounds in aqueous solutions, this approach is promising to reduce the energy consumption of the modification process.

Currently, the use of N-containing compounds as ammonia-assisted reducing agents to promote the generation of oxygen vacancies in mullite and their

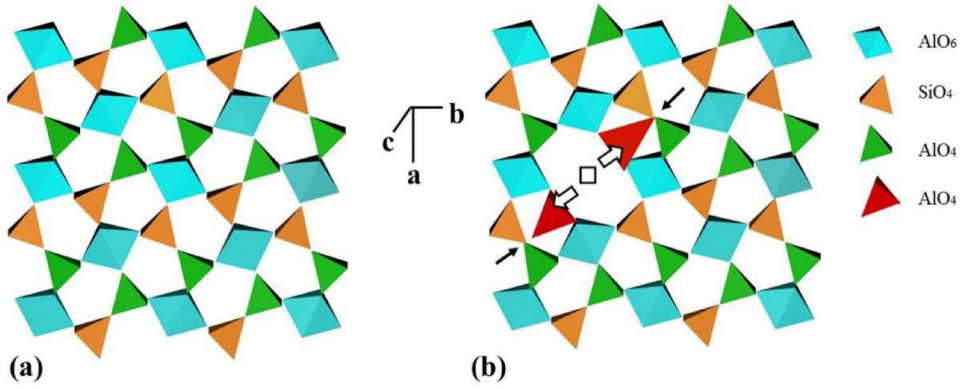

Figure 1. Crystal structure of mullite as derived from that of sillimanite. View down the c-axis of (a) sillimanite and (b) mullite. Arrows show the structural modifications in going from sillimanite to mullite: big arrows indicate the migration directions of T cations, thin arrows point to the bridging O atom (usually designated as O*) becoming a tricluster O in mullite; $\square =$ oxygen vacancy (from Fischer and Schneider) [14].

application in the adsorption of heavy metals during the co-combustion of coal and biomass is relatively underexplored. Therefore, conducting in-depth research on the modification methods of mullite and its adsorption characteristics of heavy metals during the co-combustion of coal and biomass is of significant scientific significance and practical application value. This study is expected to reveal its potential applications and advantages in the field of pollutant control and provide new solutions for the treatment of heavy metal pollution.

In the modification of aluminosilicates such as kaolin, N-containing compounds including hydrazine, urea, and formamide have been employed; this modification process is characterized by its mild conditions and ease of implementation (aqueous solutions at 100 °C) [39,40]. Should analogous methods prove effective for the modification of mullite, it could not only lead to reduced energy consumption but also serve as a reference for future technological advancements. In this study, mullite was surface-modified using formamide (F), urea (U), and ammonium acetate (AA) as modifiers. The modified mullite was used as an additive in a tubular furnace experiment to investigate its enrichment effect on Cr, Cu, Mn, Ni, Pb and Zn. The research findings will provide a theoretical basis and practical guidance for reducing heavy metal emissions in biomass and coal co-combustion projects, while also advancing the development of sustainable energy utilization and environmental protection.

2. Materials and methods

2.1. Materials

The coal and biomass used in this study were lignite coal and eucalyptus wood obtained from a coal plant in Hezhou City, Guangxi Province, China. The materials obtained were dried at a constant temperature (105 °C) until reaching a stable weight. Subsequently, the dried coal and biomass were ground and sieved through an 80-mesh (<318 μm) screen before being stored in a sealed bag for subsequent experiments. The mullite (Fuchen), formamide (Fuyu Chemical, China), urea (Tianjin Zhiyuan, China), and ammonium acetate (Macklin, China) used were all analytically pure.

2.2. Synthesis of modified mullite

The preparation process varied depending on the state of the modifier. For formamide (F), 5 g of mullite was combined with 50 mL of saturated formamide solvent and agitated in a water bath at 30 °C, 60 °C, and 90 °C for 48 hours. The mixture was rinsed and centrifuged in anhydrous ethanol to produce the mullite/formamide composite product. For urea (U) and ammonium acetate (AA), a beaker was filled with 5 g of mullite and ammonium acetate/urea (mass ratio 1:1). The mixture was then diluted with 100 mL of distilled water and agitated in a water bath at three temperatures for 48 hours. The mixture was then rinsed and centrifuged with distilled water to extract the mullite/ammonium acetate and mullite/urea.

The 5 g of the above-mentioned composite materials were placed in a 300 mL beaker, mixed with water, and ultrasonicated using an ultrasonic cell disruptor (LICHEN LC-JY96-IIN,China) (30 °C/60 °C/90 °C, 5 min, 25 kHz). Subsequently, centrifugation was performed in a centrifuge at 4000 r/min. The centrifugation process was repeated three times, each involving anhydrous ethanol to wash the solid at the bottom. Finally, the solid-phase products are dried at 80 °C. The modification process of mullite is shown in Figure 2. Each sample was labelled according to its composition, and detailed numbering was provided in Table S1.

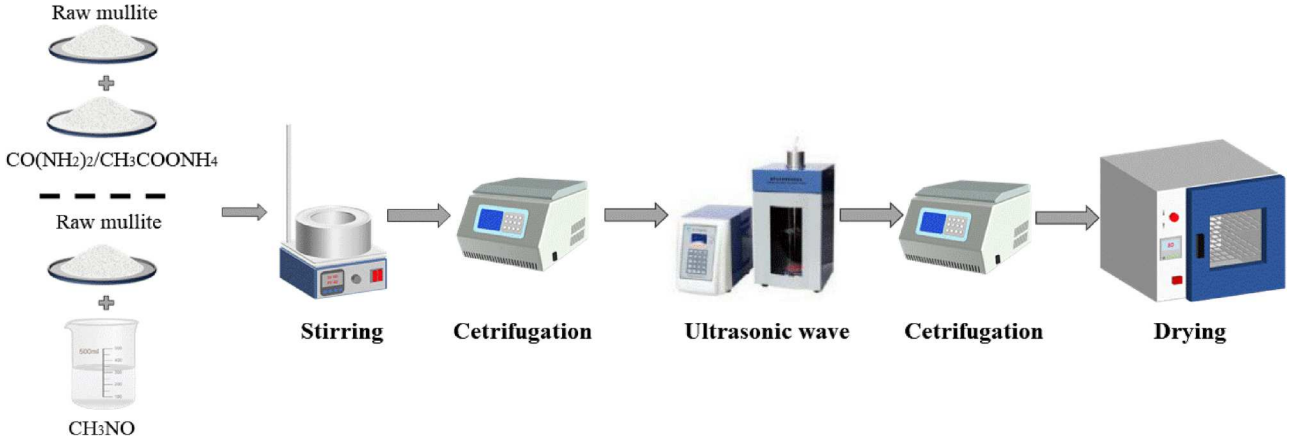

Figure 2. Process of modification mullite.

2.3. Methods

The adsorption experiments of the additives on heavy metals were conducted in a tube furnace, as shown in Figure 3, with the diameter and length of the heating tube being 50mm and 1100mm, respectively. First, introduce air at a flow rate of 1 L/min and heat the tubular furnace to 900°C. Maintain this temperature to adhere to the experimental conditions. Then, push the combustion boat with 1 g of sample (with additive ratios of 5% or 10%, and a coal-to-biomass mass ratio of 7:3, thoroughly mixed) into the centre of the quartz tube. All samples were combusted for 30 min at a constant temperature of 900 °C.

The ash samples obtained by combustion were subjected to digestion using a mixed-acid digestion system of HNO_3+H_2O_2+HCl. After digestion, the digested solution was filtered and brought to a constant volume. The solution was then analyzed for heavy metal element concentration using Inductively Coupled Plasma Optical Emission Spectroscopy (ICP-OES 5100, Agilent Technologies, USA). All experiments were performed at least twice, and the average of the duplicate experiments was taken. The effectiveness of the additives in reducing heavy metal emissions was evaluated based on the retention rate (D) and the relative enrichment factor (R). The calculation formulas for D and R are given in Eq. 1 and Eq. 2, respectively:

$$D = \frac{X_j m_1}{X m} \quad (1)$$

$$R = \frac{M_n}{M_a} \times 100\% \quad (2)$$

Where m_1 indicates the mass of coal ash; X is the total concentrations of heavy metal elements (X) in fuel; m indicates the mass of fuel; and X_j refers to the total concentrations of heavy metal elements (X) in ash following the addition of additive (j). As can be seen from the definition of D, a bigger D denotes a higher relative amount of heavy metal components in coal ash and suggests that the additive has a better adsorption impact on those metals.

Where M_a represents the heavy metal concentrations in coal ash (mg/kg) prior to adding additives, and M_n represents the heavy metal concentrations in coal ash (mg/kg) following the addition of additives. When R > 1, adding additives promotes the enrichment of heavy metals; when R < 1, on the other hand, adding additives prevents the enrichment of heavy metals.

2.4. Characterization

The crystal structures of the above samples were analyzed by X-ray diffraction (XRD, Rigaku SmartLab SE, Japan). The test of XRD used 40 mA in the scanning range from 5° to 65° and the Cu Kα (λ = 0.154056 nm) radiation at 40 kV. The adsorption and desorption of N_2 experiments were carried on the automatic adsorption apparatus (Micromeritics ASAP 2460,USA). The Brunauer-EmmettTeller (BET) with Barrett-Joyner-Halenda (BJH) method was utilized to test the specific surface area and surface pore size of the obtained samples. The morphology of the obtained sample was observed by scanning electron microscopy (SEM, Merlin, Zeiss, Germany). Fourier transform infrared spectroscopy (FT-IR, Thermo Scientific iN10, USA) was utilized to analyze the functional groups of the above samples. The FTIR spectra were recorded in the 400–4000 cm^{-1} wavenumber range.

2.5. Statistical analysis

The data were processed using Statistical Product and Service Solutions (SPSS) 27.0 software (IBM Corp., Armonk, NY, USA). The Spearman's correlation coefficient was utilized to analyze the correlation. A significance level of $P < 0.05$ was considered statistically significant.

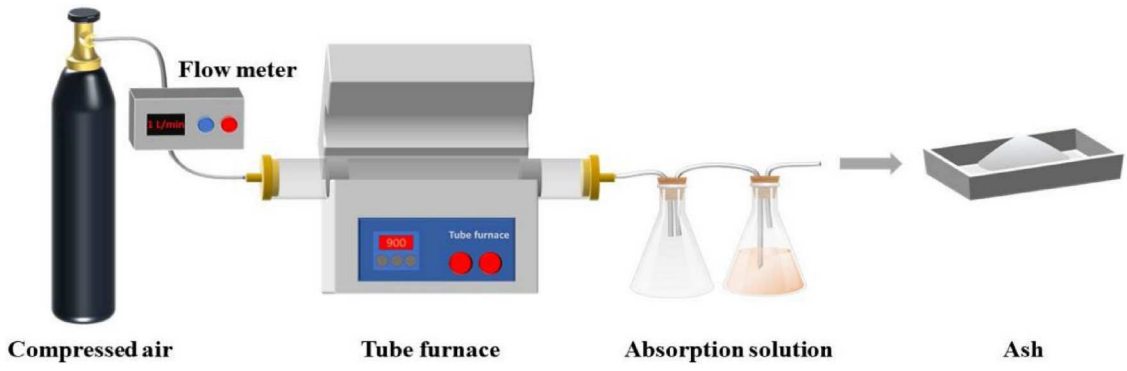

Figure 3. Schematic diagram of tubular furnace.

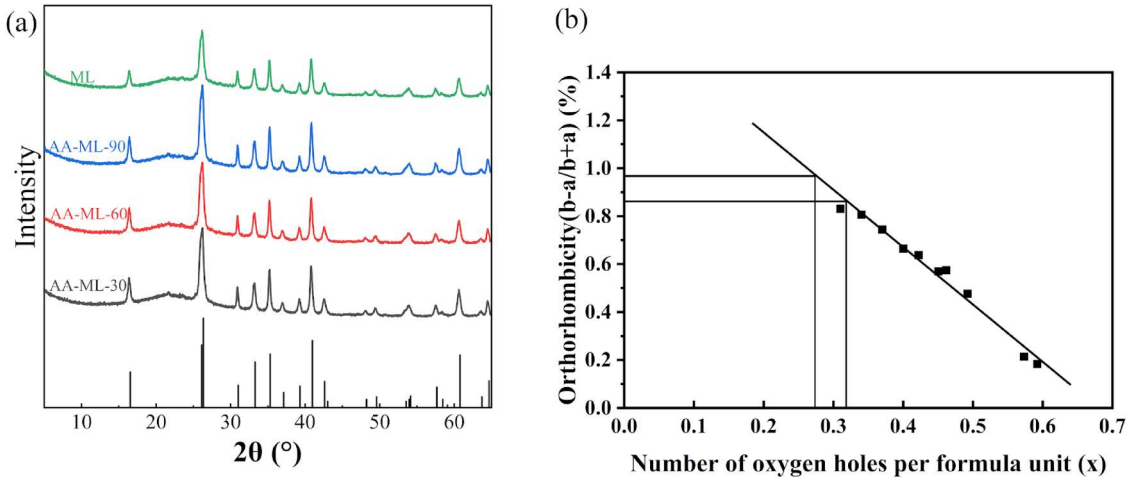

Figure 4. (a). XRD of mullite and modified mullite;(b)Variation of the orthorhombicity as a function of oxygen vacancies content (x) per formula unit in $Al_{4+2x}Si_{2-2x}O_{10-x}$, calculated from another work [45].

3. Result and discussion

3.1. Characterization analysis

3.1.1. Analysis of crystal structure

Figure 4 and Fig. s1 display the XRD spectra of the original and modified mullite, respectively. The distinctive mullite peaks may be seen at $2\theta = 16.42°$, 26.26°, 35.22°, and so forth. Good symmetry, a sharp peak shape, and well-defined kurtosis collectively indicate a high level of sample purity. In the XRD patterns, the modified mullite does not show any new characteristic peaks compared to the original mullite, indicating that the modifier has been completely removed during the modification process and has not been doped or adhered to the mullite structure.

According to the curve given by previous studies [41], an orthorhombicity parameter [42] is calculated, which is defined as $100 \times (b-a)/(b+a)$, showing the variation of lattice parameters as a function of the hole concentration x. Figure 3(b) reports the variation in orthorhombicity as a function of x. The linear variation demonstrates how the mullite's basis (a,b) planes are impacted by the relaxation brought on by hole development. The measured lattice parameters and corresponding oxygen vacancy concentrations for the samples are presented in Table 1. The orthorhombicity parameter of the mullite is 0.922, corresponding to an x of 0.294. Its chemical formula is $Al_{4.588}Si_{1.703}O_{9.703}$, and it contains 71.56 wt% Al_2O_3. The modified mullite exhibits varying degrees of increased oxygen vacancy concentrations. Among them, U-ML-60 and AA-ML-60 have achieved relatively high x-values of 0.321 and 0.319, respectively. The content of Al_2O_3 in U-ML-60 is 72.3 wt%, while AA-ML-60 contains 72.25 wt% Al_2O_3. From these XRD results, it can be inferred that the modified mullite is composed of AlO_6 octahedra, Al_2O_3 tetrahedra and SiO_2 tetrahedra.,only slightly more enriched with Al_2O_3 than those corresponding to mullite. Therefore, it can be concluded that the modification process leads to the following reactions in mullite: $2Si^{4+}+O^{2-}\rightarrow 2Al^{3+}+\square$, increasing the content of Al_2O_3 in the sample, enhancing the oxygen vacancy in the lattice structure, and providing more space for the adsorption of heavy metals. Meanwhile,Al^{3+} ions replacing Si^{4+} in the silicate tetrahedra result in mullite carrying a negative charge [27], which enables metal ions to be adsorbed by mullite through electrostatic binding.

Table 1. The XRD analysis for mullite and modified mullite.

	Lattice parameters			
Samples	a	b	c	x
F-ML-30	7.554	7.691	2.883	0.303
U-ML-30	7.560	7.696	2.888	0.308
AA-ML-30	7.553	7.690	2.887	0.303
F-ML-60	7.565	7.697	2.888	0.318
U-ML-60	7.561	7.692	2.886	0.321
AA-ML-60	7.569	7.701	2.888	0.319
F-ML-90	7.552	7.688	2.881	0.304
U-ML-90	7.564	7.699	2.889	0.310
AA-ML-90	7.557	7.690	2.882	0.315
ML	7.566	7.707	2.891	0.294

3.1.2. Analysis of BET

Table 2 shows the BET structure test results of these 4 types of mullite. Compared with the original mullite, the modified mullite has a similar specific surface area. At 30 °C and 60 °C, the specific surface area of the modified mullite follows the trend of F-ML < UU-ML < AA-ML, while at 90 °C, the trend is AA-ML < UU-ML < F-ML. This may be related to the instability of the internal structure of modified mullite at higher temperatures. Additionally, the pore size of the modified mullite has

Table 2. BET of mullite and modified mullite.

Samples	BET surface area (m^2/g)	Pore size (nm)	Pore volume (cm^3/g)
F-ML-30	5.5511	13.5932	0.018864
U-ML-30	5.9415	13.7428	0.020413
AA-ML-30	6.0794	12.4452	0.018915
F-ML-60	5.9085	13.6947	0.020229
U-ML-60	5.9139	11.9595	0.017682
AA-ML-60	6.3586	20.1361	0.032009
F-ML-90	7.5582	14.1793	0.026793
U-ML-90	6.3271	12.8040	0.020253
AA-ML-90	5.8075	13.0941	0.019011
ML	6.6456	11.7284	0.019485

increased in comparison to the original mullite, and it does not exhibit a distinct regular pattern. The performance of pore volume also lacks regularity. Most notably, AA-ML-60 stands out with a pore size of 20.1361 nm and a pore volume of 0.0320 cm^3/g, which are 1.72 and 1.64 times that of ML, respectively. The process of modification has brought about substantial alterations to the microstructure of this sample. The larger pore size and abundant porous structure can provide a richer physical space for heavy metals adsorption, thereby enhancing the physical adsorption performance of mullite.

Furthermore, an increased number of active sites are exposed to chemical adsorption when the modifier is ammonium acetate and the modification temperature is set at 60°C. This indicates that under these conditions, the modified mullite is most conducive to the development of a porous structure.

3.1.3. Analysis of micromorphology

In this study, the samples were characterized and observed using scanning electron microscopy (SEM) to obtain information about particle size distribution and surface morphology. As shown in Figure 5, ML appears as granular particles with agglomerated structures. The modified ML still maintains a granular morphology, but the image reveals the presence of some larger pores and collapsed layer structures. The results can be attributed to the modification process, which results in an increased number of oxygen vacancies between molecules. This decrease in surface agglomeration and enhancement of the structural characteristics of mullite. The average particle size of the measured samples is shown in Table 3. The average particle size of ML is 273.242 nm. Under the same temperature, the trend of mullite particle size variation obtained with different modifiers can be roughly summarized as AA-ML<U-ML<F-ML. Specifically, when modified at 30 °C, the average particle size of U-ML-30 is smaller than that of AA-ML-30. The increased hydrolysis rate of urea in water with rising temperature may enhance the formation effect of oxygen vacancies in mullite. The pore structure that has already been formed may be

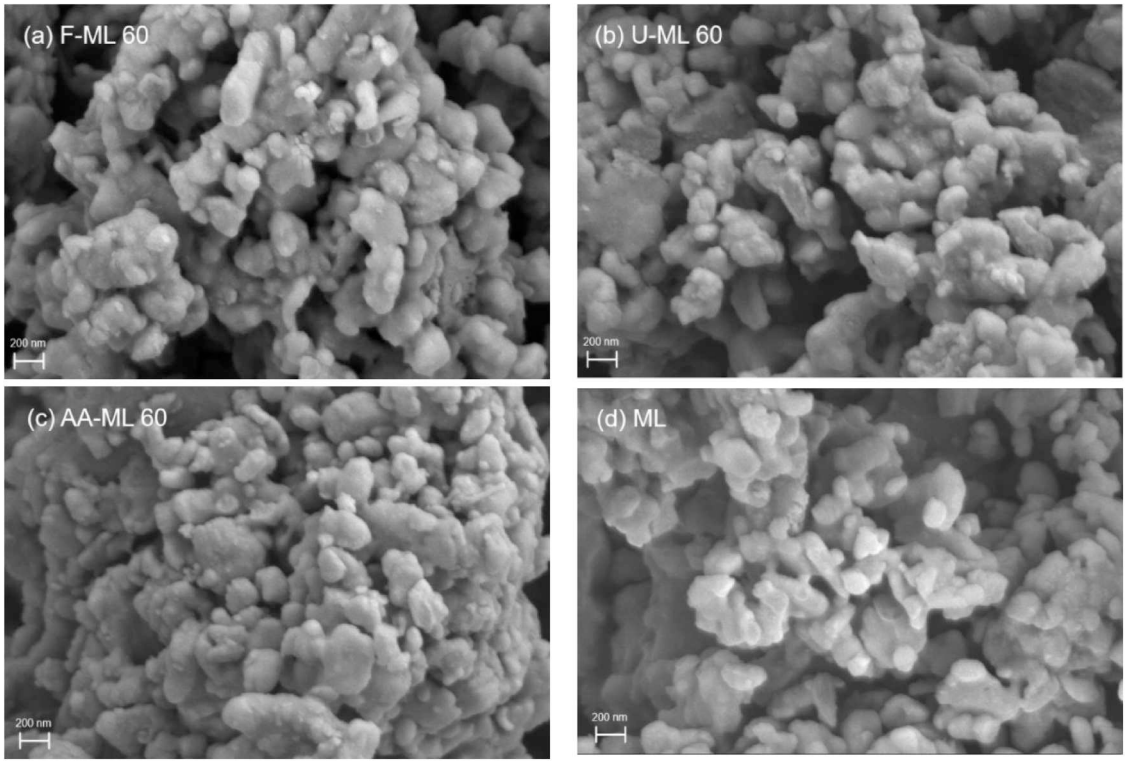

Figure 5. Micromorphology of mullite adsorbents analyzed by SEM.

Table 3. The SEM analysis for mullite and modified mullite.

Samples	Average particle size (nm)
F-ML-30	314.56
U-ML-30	285.41
AA-ML-30	301.61
F-ML-60	289.14
U-ML-60	261.99
AA-ML-60	238.93
F-ML-90	314.77
U-ML-90	293.03
AA-ML-90	271.44
ML	273.24

disrupted when exposed to boiling water at high temperatures, which can consequently affect its modification effect. It is worth noting that the average particle size of AA-ML-60 reaches the lowest among all samples at 238.93 nm. The aggregation of small particles increases the porosity of the adsorbent surface (as shown in Table 3). The improvement in surface properties is conducive to increasing the contact area between mullite and flue gas for enhanced reactivity.

3.1.4. Analysis of the functional groups

For the convenience of analyzing the primary changes in Si and Al bonds in mullite, only the infrared analysis spectra of the Si-O and Al-O bond regions are selected as shown in Figure 6, omitting the rest of the wavenumber range. The spectra of all samples are very similar, showing characteristic spectral bands of Si-O bonds in SiO_4 tetrahedra and Al-O bonds in AlO_4 tetrahedra and AlO_6 octahedra. The differences observed only in peak heights indicate that the modification process did not cause structural damage to mullite and no modifier was incorporated [43–46].

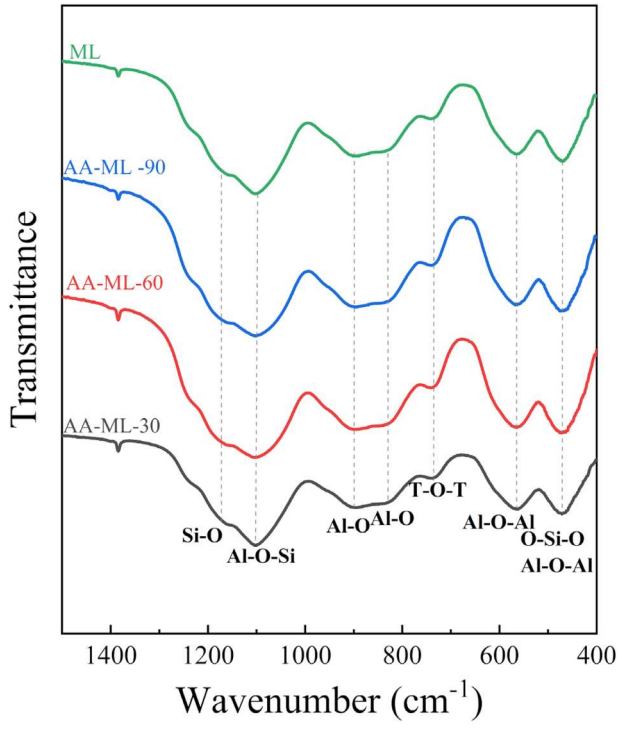

Figure 6. FTIR spectra of raw mullite and modified mullite adsorbents.

The strongest spectral band at 1103 cm^{-1} corresponds to the stretching peak of Al-O-Si, which is a characteristic peak of crystalline mullite [47]. This characteristic peak is higher in modified mullite than raw mullite, indicating that the modification process increases Al-O-Si concentration or exposes more functional groups on the surface of the sample. On the higher wavenumber side (1170 cm^{-1}), a spectral shoulder is observed, which is generated by the asymmetric stretching vibration of the Si-O bonds in the SiO_4 tetrahedra. The band at 895 cm^{-1} and the spectral shoulder at 820 cm^{-1} are related to the stretching modes of vibrations that are parallel and perpendicular to the tetrahedral chain axis of the AlO_4 tetrahedra. The weak peak around 740 cm^{-1} represents the bending vibration of the T-O-T units in the tetrahedral structure, which is significantly influenced by the T_3O triclusters. This confirms the substitution of Al for Si in the SiO_4 mullite unit, leading to the formation of oxygen vacancies and T_3O triclusters. The medium-intensity band around 564 cm^{-1} is attributed to the stretching vibration of the Al-O-Al bonds in the octahedral coordination. The medium-intensity peak around 470 cm^{-1} is influenced by the O-Si-O bending vibration of the SiO_4 tetrahedra and the Al-O-Al bending vibration of the octahedral units in mullite. This peak is considered a typical vibrational peak of mullite [43,44].

From the spectra shown in Figure 6, it is evident that the characteristic chemical bond peaks of both F-ML and AA-ML increase with the modification process. The modification of the sample has resulted in a decrease in particle size, an increase in surface area and porosity, and an enhancement in the stability of the sample structure. At the same time, the increase in the Al-O bonds of the tetrahedra in the sample compared to the Si-O bonds is more pronounced, further indicating that the modification process promotes the substitution of Al^{3+} for Si^{4+}, thereby increasing the Al_2O_3 content in the sample and forming more oxygen vacancies and adsorption sites. The peak corresponding to the T-O-T bonds is sharper and higher, indicating the formation of more tri clusters, in the sample structure, further confirming the occurrence of $2Si^{4+}+O^{2-}\rightarrow 2Al^{3+}+\square$.

3.2. Adsorption effect of modified mullite on heavy metals

In order to investigate the adsorption capacity of modified mullite for heavy metals such as Cr, Cu, Mn,

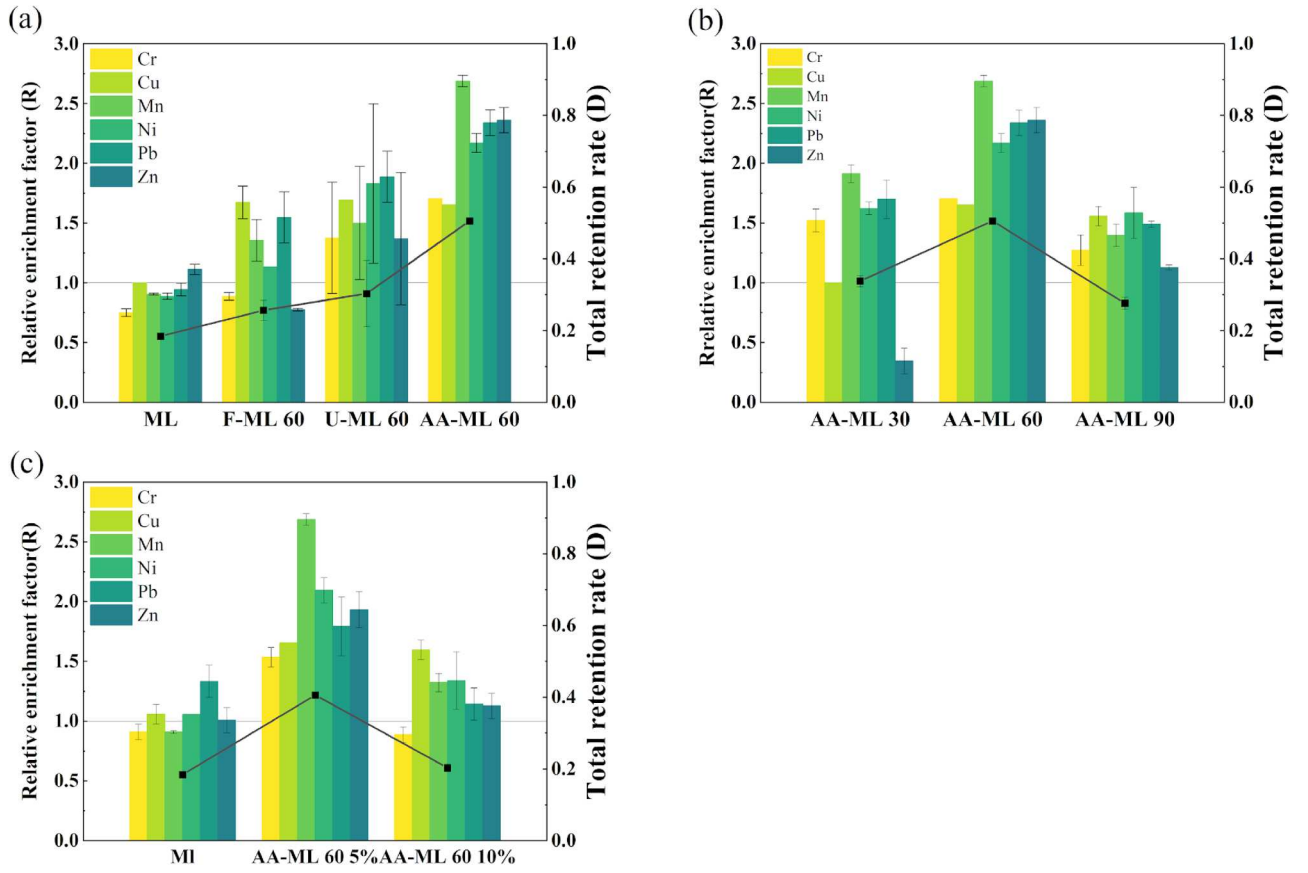

Figure 7. Relative enrichment factor (R) and retention rate (D) of heavy metals by modified mullite (a) Effect of modifiers; (b) Effect of modification temperature; (c) Effect of modifier addition ratio.

Ni, Pb, and Zn, a co-combustion experiment with coal and biomass was conducted in a tubular furnace at 900 °C, with additives added during the process. The heavy metal content in the ash residue was determined after digestion, and the adsorption performance of modified mullite for heavy metals was evaluated using the retention rate (D) and enrichment factor (R). The results are shown in Figure 7. A higher retention rate and enrichment factor indicate a more effective reduction in heavy metal emissions due to the additives.

3.2.1. Effect of modifiers

The effect of different modifiers was first investigated. Figure 7 (a) compares the adsorption performance of four types of mullite adsorbents for heavy metals in the fuel, including the original mullite and three types of modified mullite obtained by separately adding three modifiers and conducting modifications at 60 °C. It is evident that the original mullite exhibits enrichment factors for most heavy metals, which are mostly less than 1, indicating that, unexpectedly, mullite does not show enrichment effects for most heavy metals relative to pure fuel. It only exhibits enrichment effects for Zn, which may be related to the similarity in particle size between Zn^{2+} and Al^{3+} ions [48]. With the addition of modifiers, the adsorption effect of modified mullite on heavy metals becomes apparent, and it is increased relative to the original mullite. Among them, the adsorption effects of the three types of modified mullite on Cr, Mn, Ni, and Pb steadily increase from left to right. Specifically, the effect is the best when ammonium acetate is used as the modifier. The enrichment effect on Mn is particularly prominent, with an R-value reaching 2.69, which is 1.79 times higher than the original mullite's R-value of 1.5. For Cu, the effects of the three types of modified mullite are very similar. However, for Zn, F-ML-60 exhibits an inhibitory effect on its enrichment. In terms of the total content of heavy metals adsorbed by the adsorbents, both U-ML-60 and AA-ML-60 show significantly improved adsorption performance compared to the original mullite. The retention rates of heavy metals by U-ML-60 and AA-ML-60 have increased from 18.41% to 30.304% and 50.559%, respectively. This may be related to the characteristics of the three modifiers. To explain the principle behind the treatment with N-containing compounds, we referred to relevant literature [33,49]. N-containing compounds may function as reducing agents, extracting oxygen (O*) from the mullite

lattice to generate oxygen vacancies. Formamide decomposes into ammonia and carbon monoxide when boiled under normal pressure. At temperatures below 100 °C, the -NH_2 group of formamide exhibits reducing properties, potentially participating in a dehydrogenation reaction with O*. N-containing species are formed and adsorbed on unsaturated surface sites before being later removed during the ultrasonic treatment stage. Urea, an organic compound, ionizes only minimally in water, with the majority existing in its molecular form. Urea begins to hydrolyze at 60 °C, with the hydrolysis rate accelerating as the temperature reaches 80 °C and showing a significant increase above 145 °C, ultimately decomposing into NH_3 and CO_2. However, at 80 °C, urea hydrolyzes only 0.5% within one hour. The ammonia gas produced from ionization may react with lattice oxygen (O*) in a reduction reaction, leading to the removal of O* and the formation of oxygen vacancies. Ammonium acetate is a strong electrolyte, existing in water as NH_4^+ and CH_3COO^- ions. Heating accelerates the hydrolysis of NH_4^+ and CH_3COO^- ions, resulting in the production of ammonia gas. Therefore, under the same conditions, ammonium acetate can produce more reducing units to extract O*, making it more advantageous as an ammonia-assisted agent in producing oxygen vacancies.

3.2.2. Effect of modification temperature and addition ratio

The influence of modification temperature and blending ratio on the adsorption efficiency of heavy metals by mullite is shown in Figure 7 (b) and Figure 7 (c). With the increase in temperature, the adsorption efficiency of heavy metals by the three adsorbents shows a trend of initially increasing and then decreasing. The enhancement effect of the modification is not as significant as at 60 °C, where AA-ML-30 and AA-ML-90 exhibit a decrease in the retention rate for heavy metals to 33.81% and 27.65%, respectively. Several mechanisms are related to this trend. Firstly, at lower temperatures, the decomposition rate of ammonia-assisted agents in water is slow, which does not generate enough amino to reduce the oxygen atoms in mullite, resulting in a smaller number of oxygen vacancies in mullite. Furthermore, higher temperatures can enhance the decomposition rate of the ammonia-assisted agent, leading to a faster reaction rate of the sample and ultimately resulting in a better modification effect. However, excessively high temperatures can shorten the contact time between the sample and the modifier, reducing the modification effect. Lastly, in a water environment at higher temperatures, the micro-porous structure formed in mullite may collapse, and mullite particles may agglomerate, deterioration its physical structure as an adsorbent. This can lead to a reduced availability of a larger specific surface area and reactive sites for adsorption.

As the blending ratio of AA-ML-60 adsorbent increases, the adsorption efficiency of heavy metals also shows a trend of initially increasing and then decreasing. When the blending ratio is 5%, the enrichment factor of the adsorbent for each metal is greater than 1, and the total amount of heavy metal adsorption is highest. This phenomenon may be attributed to several factors. Firstly, an excess of mullite particles may aggregate during the combustion process, forming clusters or agglomerates, thereby reducing the effective contact surface area between the particles and diminishing the adsorption efficiency of heavy metals. Secondly, an increase in the blending ratio of the adsorbent leads to an increased number of available adsorption sites on its surface. However, other non-target substances may also bind to these sites simultaneously, resulting in a competitive adsorption process between heavy metal ions and other substances. When the competitive adsorption reaches a certain level, the actual total adsorption of heavy metals may be affected and decrease. Lastly, the blending ratio also affects the ash fusion characteristics of the fuel, thereby influencing the final adsorption performance.

3.3. Correlation analysis of heavy metal retention rate with x and average particle size

In this study, a correlation analysis was conducted on the samples using Spearman rank correlation, aiming to investigate the potential relationship between the adsorption capacity of mullite adsorbents and their crystal structure and microstructure. The results (as shown in Table 4) revealed a positive correlation

Table 4. Analyses on correlation of x and average particle size with a retention rate of heavy metal.

		Retention rate	x	Average particle size
Retention rate	r	1.000	/	/
	P-value	0.000	/	/
x	r	0.578	1.000	/
	P-value	0.080	0.000	/
Average particle size	r	−0.564	−0.620	1.00
	P-value	0.090	0.056	0.00

between the retention rate of heavy metals and the oxygen vacancy content (x) (r = 0.578) and a negative correlation with the average particle size (r = -0.564). This indicates that the adsorption capacity of mullite adsorbents is more strongly correlated with the oxygen vacancy content of the crystals than with the average particle size. However, both *p*-values were greater than 0.05, failing to reach statistical significance. This suggests a certain degree of correlation between the two variables, but the significance of this relationship remains undetermined. There are several possible explanations for the low significance of the correlation results. Firstly, the sample size may have been insufficient to capture the potential correlation. Secondly, measurement errors during the data collection process may have impacted the accuracy of the results. Additionally, unaccounted confounding variables may have interfered with the interpretation of the results. Nonetheless, this finding remains of significant importance. It suggests that there may be some degree of association between adsorption efficiency and the crystal structure and microstructure of the adsorbents, albeit not statistically significant. Future research could take measures to validate our results further. This contribution will enhance the comprehensive understanding of the phenomenon being studied and establish a more dependable foundation for future research.

4. Conclusion

This study aimed to modify mullite using formamide, urea, and ammonium acetate as modifiers and comprehensively characterized the modified mullite using techniques such as XRD, BET, SEM, and FTIR. Subsequently, the original mullite and the modified mullite were used as additives in a tube furnace combustion experiment to investigate their enrichment effect on heavy metals. The characterization results revealed significant changes in the microstructure of mullite after modification. The modified mullite exhibited smaller particle sizes, increased exposure to active sites on the surface, and higher concentrations of Al^{3+} ions and oxygen vacancies within the particles. The tube furnace experiment demonstrated that the modification process greatly enhanced the enrichment effect of mullite on heavy metals. Particularly when ammonium acetate was used as the modifier, the mullite modified at 60 °C (AA-ML-60) showed the best adsorption performance at an addition rate of 5%. Consequently, it can be concluded that the modification treatment of mullite can improve its adsorption efficiency. Based on the characterization data, it is speculated that the concentration of internal oxygen vacancies is the primary factor influencing the adsorption efficiency, followed by particle size (particle diameter). However, due to in-situ adsorption, it is difficult to recover the adsorbent after the experiment, which limits our ability to study its regeneration. This is a shortcoming of our current research. In the future, we will explore ways to address this issue and aim to generate more comprehensive data.

In conclusion, the modified mullite shows great potential as an effective adsorbent in the co-combustion process of coal and biomass, positively contributing to reducing heavy metal emissions from power plants.

Disclosure statement

The authors declare that they have no known competing financial interests or personal relationships that could have appeared to influence the work reported in this paper.

Funding

This work was supported by the Guangxi Key Research and Development Natural Science Foundation (GUIKEAB22035033) and the Fundamental Research Funds for the Central Universities (2022ZFJH04).

Data availability statement

The authors confirm that the data supporting the findings of this study are available within the article [and/or its supplementary materials].

ORCID

Zhaosheng Yu http://orcid.org/0000-0002-2311-4030
Xiaoqian Ma http://orcid.org/0000-0001-5829-6092

References

[1] Khorshidi Z, Ho MT, Wiley DE. Techno-economic study of biomass co-firing with and without CO2 capture in an Australian black coal-fired power plant. Energy Procedia. 2013;37:6035–6042.
[2] Demirbaş A. Biomass co-firing for boilers associated with environmental impacts. Energy Sources. 2005;27:1385–1396.
[3] Dong C, Yang Y, Yang R, et al. Numerical modeling of the gasification based biomass co-firing in a 600 MW pulverized coal boiler. Applied Energy. 2010;87:2834–2838.
[4] Riaza J, et al. Ignition and NO emissions of coal and biomass blends under different oxy-fuel atmospheres. Energy Procedia. 2013;37:1405–1412.
[5] Al-Naiema I, Estillore AD, Mudunkotuwa IA, et al. Impacts of co-firing biomass on emissions of particulate matter to the atmosphere. Fuel. 2015;162:111–120.
[6] Loeffler D, Anderson N. Emissions tradeoffs associated with cofiring forest biomass with coal: A case study in Colorado, USA. Applied Energy. 2014;113:67–77.

[7] Van Jaarsveld JGS, Van Deventer JSJ, Lorenzen L. The potential use of geopolymeric materials to immobilise toxic metals: Part I. Theory and applications. Minerals Engineering. 1997;10:659–669.
[8] Chen Q, et al. Comparison of heavy metal removals from aqueous solutions by chemical precipitation and characteristics of precipitates. J Water Process Eng. 2018;26:289–300.
[9] Ali RM, Hamad HA, Hussein MM, et al. Potential of using green adsorbent of heavy metal removal from aqueous solutions: Adsorption kinetics, isotherm, thermodynamic, mechanism and economic analysis. Ecological Engineering. 2016;91:317–332.
[10] Barakat MA, Schmidt E. Polymer-enhanced ultrafiltration process for heavy metals removal from industrial wastewater. Desalination. 2010;256:90–93.
[11] Burakov AE, et al. Adsorption of heavy metals on conventional and nanostructured materials for wastewater treatment purposes: A review. Ecotoxicology and Environmental Safety. 2018;148:702–712.
[12] Li C, Duan H, Wang X, et al. Fabrication of porous resins via solubility differences for adsorption of cadmium (II). Chemical Engineering Journal. 2015;262:250–259.
[13] Loganathan P, et al. Modelling equilibrium adsorption of single, binary, and ternary combinations of Cu, Pb, and Zn onto granular activated carbon. Environ Sci Pollut Res. 2018;25:16664–16675.
[14] Tan P, et al. Adsorption of Cu^{2+}, Cd^{2+} and Ni^{2+} from aqueous single metal solutions on graphene oxide membranes. Journal of Hazardous Materials. 2015;297:251–260.
[15] Andrejkovičová S, et al. The effect of natural zeolite on microstructure, mechanical and heavy metals adsorption properties of metakaolin based geopolymers. Applied Clay Science. 2016;126:141–152.
[16] Manfredini T, Hanuskova M. Natural raw materials in 'Traditional' ceramic manufacturing. J Univ Chem Technol Metall. 2012;47:465–470.
[17] Schneider H, Schreuer J, Hildmann B. Structure and properties of mullite—A review. Journal of the European Ceramic Society. 2008;28:329–344.
[18] Ban T, Okada K. Structure refinement of mullite by the rietveld method and a new method for estimation of chemical composition. Journal of the American Ceramic Society. 1992;75:227–230.
[19] Schneider H, Fischer RX, Schreuer J. Mullite: Crystal structure and related properties. Journal of the American Ceramic Society. 2015;98:2948–2967.
[20] Zhang Y, Wei Z, Li M, et al. Preparation and modification of Mullite whiskers/cordierite porous ceramics for Cu^{2+} adsorption and removing. ACS Omega. 2020;5:15691–15701.
[21] Agrell SO, Smith JV. Cell dimensions, solid solution, polymorphism, and identification of mullite and sillimanite. Journal of the American Ceramic Society. 1960;43:69–78.
[22] Minkina TM, et al. Sorption of Cu by chernozems in southern Russia. Journal of Geochemical Exploration. 2017;174:107–112.
[23] Tkalčec E, Gržeta B, Popović J, et al. Structural studies of Cr-doped mullite derived from single-phase precursors. Journal of Physics and Chemistry of Solids. 2006;67:828–835.
[24] Schneider H. Foreign cation incorporation in mullite. In: H Schneider, S Komarneni, editor. Mullite. Weinheim: Wiley-VCH; 2005. p. 70–93.
[25] He HP, Guo JG, Xie XD, et al. Location and migration of cations in Cu^{2+}-adsorbed montmorillonite. Environment International. 2001;26:347–352.
[26] Baldermann A, et al. Removal of heavy metals (Co, Cr, and Zn) during calcium–aluminium–silicate–hydrate and trioctahedral smectite formation. J Mater Sci. 2019;54:9331–9351.
[27] Dalacorte L, Escosteguy PAV, Bortoluzzi EC. Sorption of copper and zinc from aqueous solution by metabasalt residue and its mineralogical behavior. Water Air Soil Pollut. 2019;230:90.
[28] Zhan G, et al. The surface hydroxyl and oxygen vacancy dependent CrIJVI) adsorption performance of BiOCl. Environ Sci: Nano. 2020;7:1454–1463.
[29] Hou B, et al. Efficient removal of hexavalent chromium by nano-cerium-based adsorbent: The critical role of valence state and oxygen vacancy. Journal of Hazardous Materials. 2024;464:133020.
[30] Xu X, et al. Black $BiVO_4$: size tailored synthesis, rich oxygen vacancies, and sodium storage performance. J Mater Chem A. 2020;8:1636–1645.
[31] Kim B-S, Bae J, Jeong H, et al. Surface restructuring of supported nano-ceria for improving sulfur resistance. ACS Catal. 2021;11:7154–7159.
[32] Li G, et al. Defect enhanced CoMnNiOx catalysts derived from spent ternary lithium-ion batteries for low-temperature propane oxidation. Applied Catalysis B: Environmental. 2022;309:121231.
[33] Liu D, et al. Understanding the nature of ammonia treatment to synthesize oxygen vacancy-enriched transition metal oxides. Chem. 2019;5:376–389.
[34] Xiao M, et al. Molten-salt-mediated synthesis of an atomic Nickel co-catalyst on TiO_2 for improved photocatalytic H_2 evolution. Angewandte Chemie International Edition. 2020;59:7230–7234.
[35] Xiang K, et al. Two dimensional oxygen-vacancy-rich Co_3O_4 nanosheets with excellent supercapacitor performances. Chem Commun. 2017;53:12410–12413.
[36] Xu Y, Qu Z, Ren Y, et al. Enhancement of toluene oxidation performance over Cu–Mn composite oxides by regulating oxygen vacancy. Applied Surface Science. 2021;560:149983.
[37] Sun M, et al. Enhanced catalytic performance by oxygen vacancy and active interface originated from facile reduction of OMS-2. Chemical Engineering Journal. 2018;331:626–635.
[38] Gao R, et al. Enhancing the catalytic activity of Co_3O_4 nanosheets for Li-O_2 batteries by the incorporation of oxygen vacancy with hydrazine hydrate reduction . Inorg Chem. 2019;58:4989–4996.
[39] Zhang X, et al. Improved sodium adsorption by modified kaolinite at high temperature using intercalation-exfoliation method. Fuel. 2017;191:198–203.
[40] Prabawa ID, Lestari RY, Hamdi S. Modified physical properties of kaolin by intercalation and exfoliation method. IOP Conf Ser: Mater Sci Eng. 2020;980:012009.
[41] Cameron WE. Mullite:a substituted alumin. American Mineralogist. 1970;62:747–755.

[42] Gomes S, François M. Characterization of mullite in silicoaluminous fly ash by XRD, TEM, and 29Si MAS NMR. Cement and Concrete Research. 2000;30:175–181.
[43] Ritz M. Infrared and Raman Spectroscopy of Mullite Ceramics Synthesized from Fly Ash and Kaolin. Minerals. 2023;13:864.
[44] Voll D, Angerer P, Beran A, et al. A new assignment of IR vibrational modes in mullite. Vibrational Spectroscopy. 2002;30:237–243.
[45] Zhang Y-F, Lei X-R, Chen A-Z, et al. Study on Mullite formation mechanism in Acid and Alkaline. Bull Chin Ceram Soc. 2011;30:904–908.
[46] Beran A, Voll D, Schneider H. Dehydration and structural development of mullite precursors: an FTIR spectroscopic study. Journal of the European Ceramic Society. 2001;21:2479–2485.
[47] Padmaja P, Anilkumar GM, Mukundan P, et al. Characterisation of stoichiometric sol–gel mullite by Fourier transform infrared spectroscopy. International Journal of Inorganic Materials. 2001;3:693–698.
[48] Chen C-S, Chou C-C, Chang S-W, et al. First-principles study on variation of lattice parameters of mullite $Al_{4+2x}Si_{2-2x}O_{10-x}$ (x = 0.125, 0.250, 0.375). American Mineralogist. 2010;95:1617–1623.
[49] Zhan F, et al. A comprehensive review of oxygen vacancy modified photocatalysts: synthesis, characterization, and applications. Phys Chem Chem Phys. 2024;26:11182–11207.